Structural Analysis of Historical Constructions, New Delhi 2006
P.B. Lourenço, P. Roca, C. Modena, S. Agrawal (Eds.)

Homogenisation Approaches for Structural Analysis of Masonry Buildings

Paulo B. Lourenço
University of Minho, Department of Civil Engineering, Guimarães, Portugal

Alberto Zucchini
ENEA, FIS.MET, Bologna, Italy

Gabriele Milani and Antonio Tralli
University of Ferrara, Department of Civil Engineering, Ferrara, Italy

ABSTRACT: Modern methodologies for the conservation of architectural heritage require structural analysis for the purpose of diagnosis and safety evaluation. This is not an easy task, as masonry structures usually feature a very low tensile strength, thus rendering the tool usually adopted for design of new structures (linear elastic analysis) of very limited use. Non-linear analysis of ancient masonry structures is a popular field in masonry research and homogenisation techniques play presently a major role, despite the mathematical and conceptual difficulties inherent to the approach. The paper addresses different homogenisation techniques available in the literature, with a focus on micro-mechanical models and on the polynomial expansion of the stress field. These seem promising and accurate strategies for advanced structural analysis.

1 INTRODUCTION

Masonry is a heterogeneous material that consists of units and joints. Units are such as bricks, blocks, ashlars, adobes, irregular stones and others. Mortar can be clay, bitumen, chalk, lime/cement based mortar, glue or other. The huge number of possible combinations generated by the geometry, nature and arrangement of units as well as the characteristics of mortars raises doubts about the accuracy of the term “masonry”. Still, much information can be gained from the study of regular masonry structures, in which a periodic repetition of the microstructure occurs due to a constant arrangement of the units (or constant bond).

The difficulties in performing advanced testing of this type of structures are quite large due to the innumerable variations of masonry, the large scatter of *in situ* material properties and the impossibility of reproducing it all in a specimen. Therefore, most of the advanced experimental research carried out in the last decades concentrated in brick / block masonry and its relevance for design. Accurate modelling requires a comprehensive experimental description of the material, which seems mostly available at the present state of knowledge, see e.g. CUR (1997) and Lourenço (1998) for a review.

The global field of structural analysis of masonry structures encompasses several different approaches and a comprehensive review is given in Lourenço (2002). The present paper focuses exclusively on the analysis of masonry structures making use of homogenisation techniques. This is an item that has received a growing interest from the scientific committee, being rooted in a very strong community, mostly oriented to composites and, more recently, to problems involving micro-scale phenomena. As an example, on July 17, 2006, 10,199 articles could be found in the Web of Science® regarding homogenisation. This compares to only 1,807 articles about masonry. From these, 80 papers (3.3%) address the issue of masonry homogenisation, which is a relevant number taking into account that the subject is relatively new in the masonry community.

2 ON THE MODELLING MASONRY STRUCTURES

In general, the approach towards the numerical representation of masonry can focus on the micro-modelling of the individual components, *viz.* unit (brick, block, etc.) and mortar, or the macro-modelling of masonry as a composite, Rots (1991). Depending on the level of accuracy and the simplicity desired, it is possible to use the following modelling strategies, see Fig. 1:

- Detailed micro-modelling - units and mortar in the joints are represented by continuum elements whereas the unit-mortar interface is represented by discontinuum elements;
- Simplified micro-modelling - expanded units are represented by continuum elements whereas the behaviour of the mortar joints and unit-mortar interface is lumped in discontinuum elements;
- Macro-modelling - units, mortar and unit-mortar interface are smeared out in a homogeneous continuum.

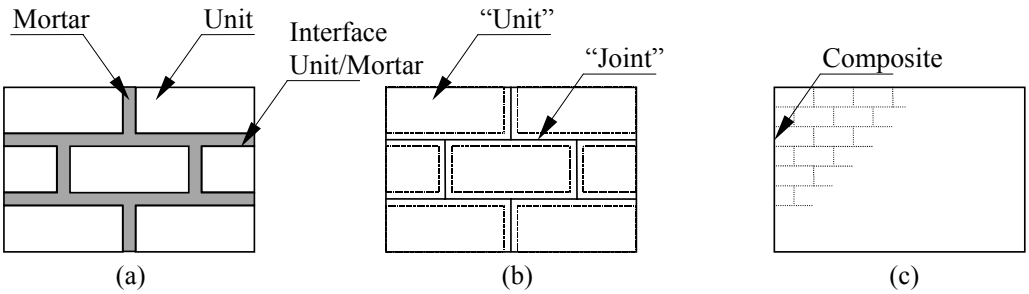

Figure 1 : Modelling strategies for masonry structures: (a) detailed micro-modelling; (b) simplified micro-modelling; (c) macro-modelling.

In the first approach, Young's modulus, Poisson's ratio and, optionally, inelastic properties of both unit and mortar are taken into account. The interface represents a potential crack/slip plane with initial dummy stiffness to avoid interpenetration of the continuum. This enables the combined action of unit, mortar and interface to be studied under a magnifying glass. In the second approach, each joint, consisting of mortar and the two unit-mortar interfaces, is lumped into an average interface while the units are expanded in order to keep the geometry unchanged. Masonry is thus considered as a set of elastic blocks bonded by potential fracture/slip lines at the joints. Accuracy is lost since Poisson's effect of the mortar is not included. The third approach does not make a distinction between individual units and joints but treats masonry as a homogeneous anisotropic continuum. One modelling strategy cannot be preferred over the other because different application fields exist for micro- and macro-models. In particular, micro-modelling studies are necessary to give a better understanding about the local behaviour of masonry structures.

It is noted that different levels of sophistication can also be adopted to create structural models, namely structural component models or continuum structural models (macro-modelling approaches) and discontinuum structural models (a micro-modelling approach). Difficulties of conceiving and implementing macro-models for the analysis of masonry structures arise especially due to the intrinsic complexity of formulating anisotropic inelastic behaviour. Only a reduced number of authors tried to develop specific models for the analysis of masonry structures, e.g. Dhanasekar *et al.* (1985), Lourenço *et al.* (1998), Berto *et al.* (2002), using different inelastic criteria for tension and compression. Therefore, the homogenisation techniques shown in Fig. 2, which permit to establish constitutive relations in terms of averaged stresses and strains from the geometry and constitutive relations of the individual components, can represent a step forward in masonry modelling, mostly because of the possibility to use standard material models and software codes for isotropic materials.

The most popular homogenisation approach replaces the complex geometry of the basic cell by a simplified geometry so that a close-form solution of the homogenisation problem is possible, e.g. Pande *et al.* (1989) and Maier *et al.* (1991). The homogenisation has generally been performed in two steps, head (or vertical) and bed (or horizontal) joints being introduced successively. The use of two separate homogenisation steps does not explicitly account for the

regular offset of vertical mortar joints belonging to two consecutive layered unit courses, which results in significant errors in the case of non-linear analysis.

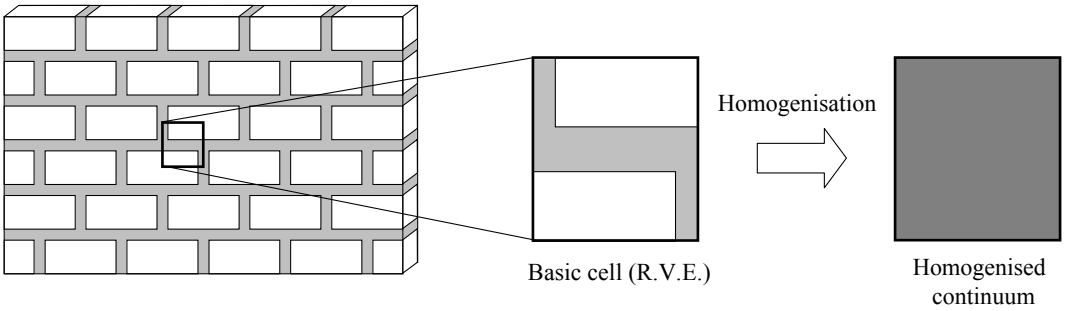

Figure 2 : Basic cell for masonry and homogenisation process.

Many other approaches involving different approximations and ingenious assumptions have been sought, with an increasing large number of papers in the recent years, e.g. Pietruszczak and Niu (1992), where a two-stage homogenization procedure was employed with the head joints considered as uniformly dispersed elastic inclusions and the bed joints assumed to represent a set of continuous weakness, or Gambarotta and Lagomarsino (1997), Massart *et al.* (2004), Podestà (2005), Calderini and Lagomarsino (2006), where simplified non-linear homogenisation techniques were used.

To overcome most of the approximation addressed above, micromechanical homogenisation approaches that consider additional internal deformation mechanisms have been derived, independently, by van der Pluijm (1999), Lopez *et al.* (1999) and Zucchini and Lourenço (2002). Another powerful approach is based on the polynomial expansion of the stress field inside the R.V.E., see e.g. Milani et al. (2006a). These two approaches are further reviewed in this paper.

3 A MICROMECHANICAL HOMOGENISATION APPROACH

3.1 Descriptive analysis of masonry

As a consequence of the differences in stiffness between units and mortar, a complex interaction between the two masonry components occurs when masonry is deformed. The differences in stiffness cause a unequal distribution of deformations over units and mortar, compared with the average deformation of masonry composite. As a result the individual (internal) stresses of units and mortar deviate from the average (external) stresses of the composite.

For the purpose of understanding the internal deformational behaviour of masonry components (units and mortar), when average deformations occur on the boundaries of the basic cell, detailed finite element calculations have been carried out for different loading conditions. For a clear discussion of the internal distribution of stresses, a right-oriented *x*-*y*-*z* coordinate system was defined, where the *x*-axis is the parallel to the bed joints, the *y*-axis is parallel to the head joints and the *z*-axis is normal to the masonry plane, see Fig. 3. This figure also shows the components considered in the approach.

A finite element calculation of the R.V.E. under homogeneous deformation was made for the purpose of validation. The mesh used in the analyses consists of 24 × 4 × 12 twenty-noded quadratic 3-D elements with reduced integration. The unit dimensions are 210 × 100 × 52 mm^3 and the mortar thickness is 10 mm. The assumption that the units are stiffer than the joints is usually made by the masonry research community. In the present analysis, in order to better understand the deformational behaviour of the mortar, the units are considered infinitely stiff (for this purpose, the adopted ratio between unit and mortar stiffness was 1000). Fig. 4 illustrates the deformation corresponding to the analysis of the basic cell under compression along the axis *x*, and under shear in the planes *xy*, *xz* and *yz*. Loading is applied with adequate tying of the nodes in the boundaries, making use of the symmetry and antisymmetry conditions appropriate to each load case. Therefore, the resulting loading might not be associated with uniform stress conditions or uniform strain conditions. Linear elastic behaviour is assumed in all cases.

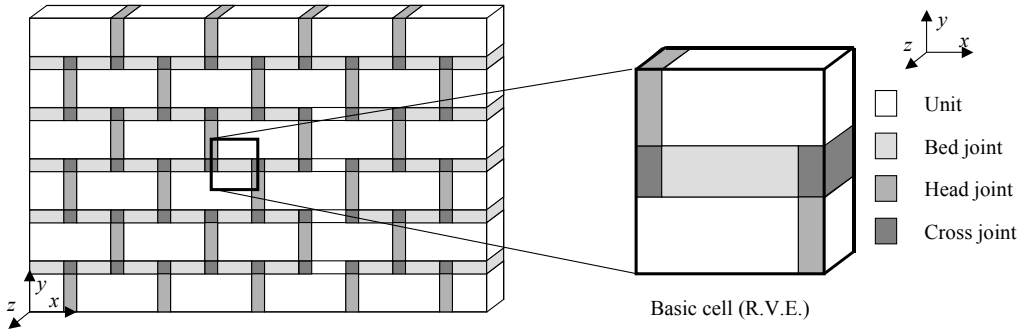

Figure 3 : Definition of masonry axes and masonry components considered in the adopted formulation: Unit, head joint, bed joint and cross joint.

Fig. 4a demonstrates that, for compression along the *x*-axis, the unit and the bed joint are mostly subjected to normal stresses, the bed joint is strongly distorted in shear and the cross joint is subjected to a mixed shear / normal stress action. While the cross joint effect can be neglected if the cross joint is small compared to the basic cell, the shear of the bed joint must be included in the micro-mechanical model of masonry for stiff units.

Fig. 4b demonstrates that, for *xy* shear, the unit and the head joint are mostly subjected to shear stresses, the bed joint is strongly distorted in the normal direction (tension) and the cross joint is subjected to a mixed shear / normal stress. Due to antisymmetric conditions, the neighbouring basic cells will feature normal compression in the bed joint. While the cross joint effect can be neglected if the cross joint is small compared to the basic cell, the normal stress of the bed joint must be included in the micro-mechanical model.

The deformation of the basic cell under *xz* shear is shown in Fig. 4c. The cell components are mostly subjected to shear stresses, with unit and head joint deformed in the horizontal plane, while the bed joint is distorted also in the vertical plane. Therefore the shear stress cannot be neglected in a micro-mechanical model. Finally, the deformation of the basic cell under *yz* shear is shown in Fig. 4d. All cell components are mainly distorted by shear in the vertical plane, while minor local stress components do not produce significant overall effects.

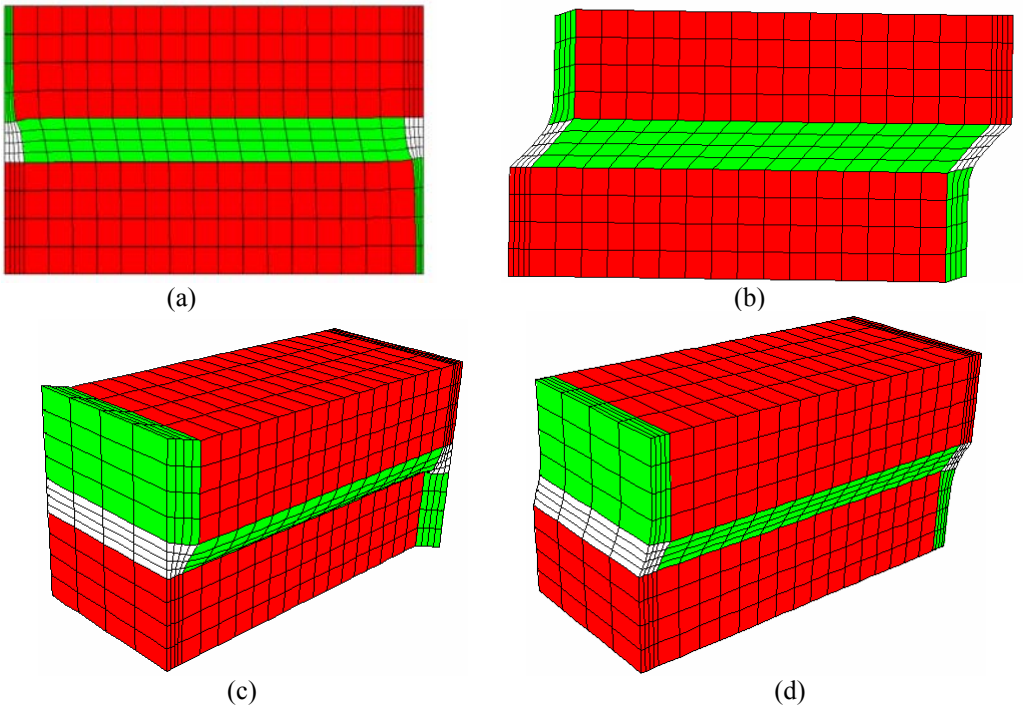

Figure 4 : Deformed configuration resulting from the finite element analysis on the basic cell: (a) compression *x*, (b) shear *xy*, (c) shear *xz* and (d) shear *yz*.

3.2 Formulation of the model

Zucchini and Lourenço (2002) have shown that the elastic mechanical properties of an orthotropic material equivalent to a basic masonry cell can be derived from a suitable micromechanical model with appropriate deformation mechanisms, which take into account the staggered alignment of the units in a masonry wall. The unknown internal stresses and strains can be found from equilibrium equations at the interfaces between the basic cell components, from a few ingenuous assumptions on the kinematics of the basic cell deformation and by forcing the macro-deformations of the model and of the homogeneous material to contain the same strain energy. This homogenisation model has already been extended with good results to non-linear problems in the case of a masonry cell failure under tensile loading parallel to the bed joint and under compressive loading, Zucchini and Lourenço (2004, 2006).

The simulation has been accomplished by coupling the elastic micro-mechanical model with a damage model for joints and units by means of an iterative solution procedure to calculate the damage coefficients. A simple isotropic damage model with only one single parameter has been utilized, because the discrete internal structure of the cell, and implicitly its global anisotropic behaviour, is taken into account by the three-dimensional micromechanical model. The geometry for the basic masonry cell and its components is shown in Fig. 5, where it can be seen that the complex geometry is replaced by four components, namely unit, bed joint, head joint and cross joint.

When the basic cell is loaded only with normal stresses, the micromechanical model of Zucchini and Lourenço (2002) assumes that all shear stresses and strains inside the basic cell can be neglected, except the in-plane shear stress and strain (σ_{xy} and ε_{xy}) in the bed joint and in the unit. The non-zero stresses and strains in the bed joint, head joint and unit are assumed to be constant, with the exception of the normal stress σ_{xx} in the unit, which is a linear function of x and accounts for the effect of the shear σ_{xy} in the bed joint, and with the exception of the shear stress σ_{xy} in the unit, which is linear in y. The coupling of this model with non-linear constitutive models, leads to an iterative algorithm, in which at each cycle a system of equilibrium equations is solved to obtain the unknown effective stresses and strains.

The governing linear system of 20 equilibrium equations in the unknown internal stresses and strains of the masonry cell, to be solved at each iteration, can be rewritten for a strain driven compression in y, as:

$$r^2\sigma_{xx}^2 = r^b\bar{\sigma}_{xx}^b - \frac{l-t}{2h}r^1\sigma_{xy}^1 \qquad \text{Interface brick-head joint} \qquad (1)$$

$$r^b\sigma_{yy}^b = r^1\sigma_{yy}^1 \qquad \text{Interface brick-bed joint} \qquad (2)$$

$$hr^2\sigma_{xx}^2 + 2tr^1\sigma_{xx}^1 + hr^b\bar{\sigma}_{xx}^b + (l-t)r^1\sigma_{xy}^1 = 0 \qquad \text{Right boundary} \qquad (3)$$

$$(h + 4t\frac{r^2}{r^1+r^2})\,\varepsilon_{yy}^2 + h\varepsilon_{yy}^b = 2(h+t)\varepsilon_{yy}^0 \qquad \text{Upper boundary} \qquad (4)$$

$$thr^2\sigma_{zz}^2 + (l-t+t\frac{r^1+r^2}{r^1})tr^1\sigma_{zz}^1 + lhr^b\sigma_{zz}^b = 0 \qquad \text{Front boundary} \qquad (5)$$

$$2t\varepsilon_{yy}^1 + h\varepsilon_{yy}^b = (4t\frac{r^2}{r^1+r^2} + h)\varepsilon_{yy}^2 \qquad \text{Upper boundary} \qquad (6)$$

$$t\varepsilon_{xx}^2 + l\bar{\varepsilon}_{xx}^b = (l-t+4t\frac{r^1}{r^1+r^2})\varepsilon_{xx}^1 \qquad \text{Right boundary} \qquad (7)$$

$$\varepsilon_{zz}^b = \varepsilon_{zz}^1 \qquad \text{Front boundary} \qquad (8)$$

$$\varepsilon_{zz}^b = \varepsilon_{zz}^2 \qquad \text{Front boundary} \qquad (9)$$

$$\varepsilon_{xx}^k = \frac{1}{E^k}\left[\sigma_{xx}^k - \nu^k\left(\sigma_{yy}^k + \sigma_{zz}^k\right)\right]$$

$$\varepsilon_{yy}^k = \frac{1}{E^k}\left[\sigma_{yy}^k - \nu^k\left(\sigma_{xx}^k + \sigma_{zz}^k\right)\right] \qquad k = b,1,2 \qquad (10)$$

$$\varepsilon_{zz}^k = \frac{1}{E^k}\left[\sigma_{zz}^k - \nu^k\left(\sigma_{xx}^k + \sigma_{yy}^k\right)\right]$$

$$\varepsilon_{xy}^{1} = \frac{\varepsilon_{xx}^{2} - \bar{\varepsilon}_{xx}^{b}}{4} - \left(\frac{l-t}{8hE^{b}} + \frac{h}{6tG^{b}}\right)\frac{r^{1}}{r^{b}}\sigma_{xy}^{1} \tag{11}$$

$$\sigma_{xy}^{1} = 2G^{1}\varepsilon_{xy}^{1} \tag{12}$$

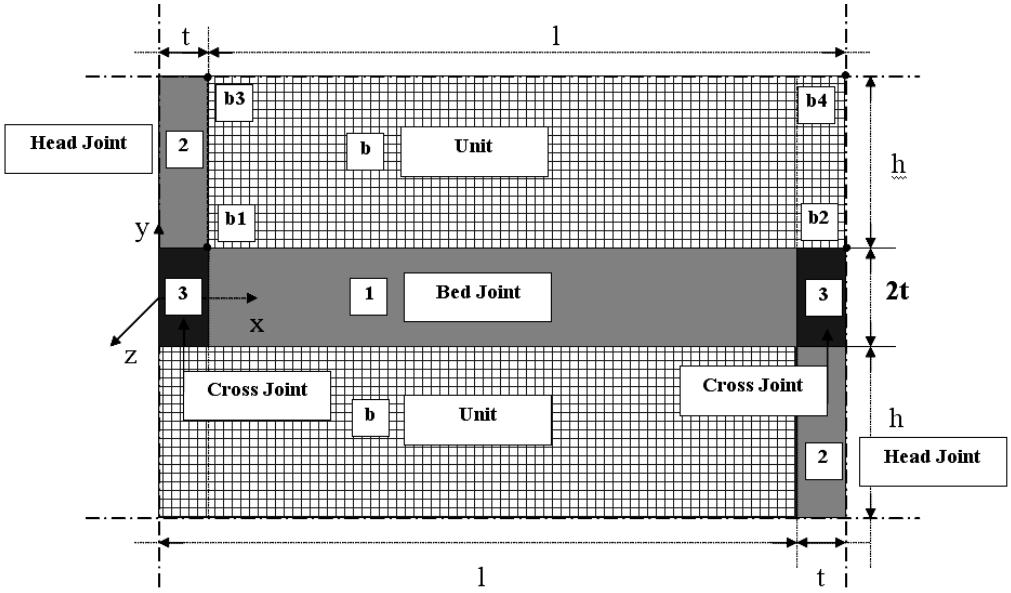

Figure 5 : Adopted geometry symbols.

As shown in Fig. 5, l is half of the unit length, h is half of the unit height and t is half of the bed joint width. Here also, E is the Young modulus, G is the shear modulus, ν is the Poisson coefficient, ε_{ij} is the strain component and σ_{ij} is the stress component. Unit, bed joint, head joint and cross joint variables are indicated throughout this paper, respectively by the superscripts b, 1, 2 and 3, according to Fig. 5. $\bar{\sigma}_{xx}^{b}$ and $\bar{\varepsilon}_{xx}^{b}$ are the mean value of the (non-constant) normal stress σ_{xx} and of the (non-constant) normal strain ε_{xx} in the unit, respectively. ε_{yy}^{0} is the uniform normal (macro) strain, perpendicular to the bed joint, on the faces of the homogenised basic cell. Finally, $r = 1 - d$, where d is the scalar damage coefficient, ranging from 0 to 1 and representing a measure of the material damage. The damaged σ_d and undamaged (or effective) stresses σ are correlated by the relation:

$$\boldsymbol{\sigma}_{d} = (1-d)\mathbf{D}\boldsymbol{\varepsilon} = (1-d)\boldsymbol{\sigma} \tag{13}$$

where $\boldsymbol{D}$ is the elastic operator.

The adopted damage model in tension, Zucchini and Lourenço (2004), is a simple scalar isotropic model, with a Rankine type damage surface:

$$\sigma_{p} = \sigma_{t} \qquad \sigma_{t} \le \sigma_{p} \le \infty \tag{14}$$

where σ_{p} is the maximum effective principal stress and σ_{t} the tensile strength of the given cell component. In the unit, where the normal stress σ_{xx}^{b} varies linearly in the x direction, the damage is controlled by the maximum principal stress in the entire unit and not by the maximum principal stress obtained with the average value $\bar{\sigma}_{xx}^{b}$.

The damage can only increase monotonically with the evolution law:

$$d = 1 - \frac{\sigma_{t}}{\sigma_{p}} e^{A\left(1-\frac{\sigma_{p}}{\sigma_{t}}\right)} \tag{15}$$

The parameter A is related to the mode I or mode II fracture energies (G^{I} and G^{II}) and strengths (σ_{t} and σ_{s}) of the material respectively by

$$A_t = \left(\frac{G^I E}{l\sigma_t^2} - \frac{1}{2} \right)^{-1} \qquad A_s = \left(\frac{G^{II} G}{l\sigma_s^2} - \frac{1}{2} \right)^{-1} \tag{16}$$

where E and G are the Young and shear moduli and l is the characteristic internal length of fracture usually adopted to obtain mesh independent results, which is assumed here to be the material dimension in the direction of the load.

The adopted model in compression, Zucchini and Lourenço (2006), is a Drucker-Prager model according to the classical formulation:

$$3k_1\sigma_m + \overline{\sigma} - k_2 = 0 \tag{17}$$

where

$$\sigma_m = \frac{\sigma_{ii}}{3} = -p\,, \qquad \overline{\sigma} = \sqrt{\frac{1}{2}\sigma_{ij}^{'}\sigma_{ij}^{'}} = \frac{q}{\sqrt{3}} \tag{18}$$

$$k_1 = \frac{2\sin\phi_f}{\sqrt{3}(3-\sin\phi_f)}, \qquad k_2 = \frac{6\cos\phi_f}{\sqrt{3}(3-\sin\phi_f)}c \tag{19}$$

and ϕ_f is the friction angle and c is the cohesion. The friction angle was assumed independent from the plastic deformation, while a bi-parabolic law in the strain hardening equivalent plastic strain $\varepsilon_{p,eq}$ is adopted for the material yield stress. The curve $\sigma_c(\varepsilon_{p,eq})$ is completely defined by the material strength σ_{c0} (the peak stress), the peak equivalent plastic strain ε_0 and the post-peak specific fracture energy g_c:

$$\begin{aligned} \sigma_c &= \frac{\sigma_{c0}}{3}\left(-2\frac{\varepsilon_{p,eq}^2}{\varepsilon_0^2} + 4\frac{\varepsilon_{p,eq}}{\varepsilon_0} + 1 \right) && 0 \le \varepsilon_{p,eq} \le \varepsilon_0 \\ \sigma_c &= \sigma_{c0}\left\{ 1 - \left[\frac{2\sigma_{c0}}{3g_c}\left(\varepsilon_{p,eq} - \varepsilon_0\right) \right]^2 \right\} && \varepsilon_0 \le \varepsilon_{p,eq} \end{aligned} \tag{20}$$

3.3 Elastic results

The model briefly described was applied to a real masonry basic cell and compared with the results of an accurate finite element analysis (FEA). In the finite element analysis and the analytical model, the properties of the components can be taken absolutely equal.

The same elastic properties have been adopted for the bed joint, head joint and cross joint ($E_1 = E_2 = E_3 = E_m$, $\nu_1 = \nu_2 = \nu_3 = \nu_m$). Different stiffness ratios between mortar and unit are considered. This allows to assess the performance of the model for inelastic behaviour. In fact, non-linear behaviour is associated with (tangent) stiffness degradation and homogenisation of non-linear processes will result in large stiffness differences between the components. In the limit, the ratio between the stiffness of the different components is zero (or infinity), once a given components has no stiffness left. The unit dimensions are 210 × 100 × 52 mm^3 and the mortar thickness is 10 mm. The material properties of the unit are kept constant, whereas the properties of the mortar are varied. For the unit, the Young's modulus E_b is 20 GPa and the Poisson's ratio ν_b is 0.15. For the mortar, the Young's modulus is varied to yield a ratio E_b / E_m ranging from 1 to 1000. The Poisson's ratio ν_m is kept constant to 0.15.

The adopted range of E_b / E_m is very large (up to 1000), if only linear elastic behaviour of mortar is considered. However, those high values are indeed encountered if inelastic behaviour is included. In such case, E_b and E_m should be understood as linearised tangent Young's moduli, representing a measure of the degradation of the (tangent / secant) stiffness matrices utilised in the numerical procedures adopted to solve the non-linear problem. Note that the ratio E_b / E_m tends to infinity when softening of the mortar is complete and only the unit remains structurally active.

The elastic properties of the homogenised material, calculated by means of the proposed micro-mechanical model, are compared in Fig. 6a with the values obtained by FE analysis. The agreement is very good in the entire range $1 \leq E_b / E_m \leq 1000$, with a maximum error ≤ 6%.

A comparison between the results obtained with the micro-mechanical model and the experimental results of Page (1981,1983) are given in Fig. 6b. Very good agreement is found in the shape of the yield surface, indicating that the proposed model can be used as a possible macro-model to represent the composite failure of masonry.

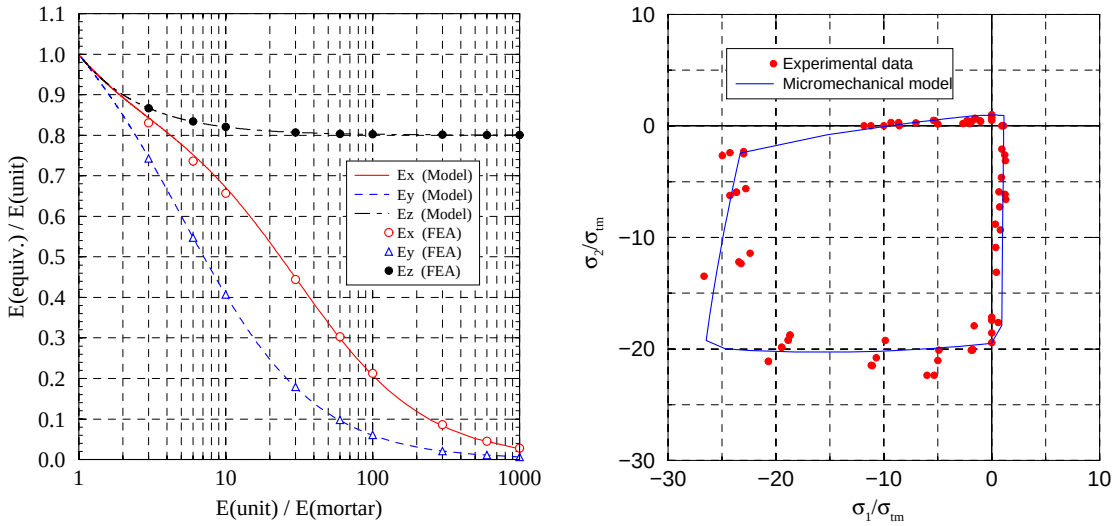

(a) (b)

Figure 6 : Elastic results for the micro-mechanical model: (a) comparison of Young's moduli with FEA results for different stiffness ratios; (b) comparison with experimental results of Page (1981,1983).

3.4 Non-linear results

The algorithm was implemented in a numerical program for the simulation of a masonry cell under normal stresses. In order to check its performance, the algorithm has been tested in the fracture problem of an infinitely long wall under tensile loading parallel to the bed joint (Fig. 7a), which has been analysed by Lourenco et *al.* (1999) with a sophisticated finite element interface model based on multisurface plasticity. This model consists of two half units in the vertical direction and of two and a half units in the horizontal direction. In the middle of the specimen a potential crack/slip line through head and bed joints is included. The unit dimensions are 900 × 600 ×100 mm^3. With the new model, only the central basic cell in the wall is represented, but such approach does not introduce any qualitative difference with the original problem, because the relation between tensile stress and crack opening is independent from the specimen length.

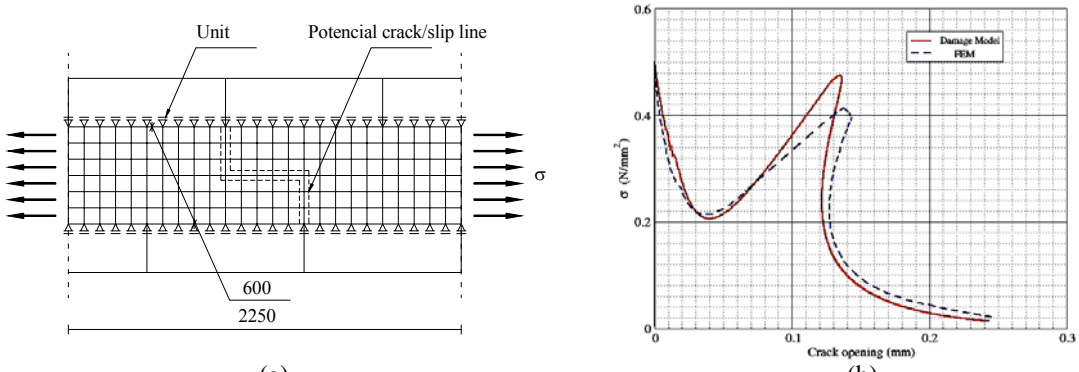

(a) (b)

Figure 7 : Inelastic response of the model in tension: (a) infinitely long masonry wall under tensile loading parallel to the bed joints; (b) stress/crack opening diagram and comparison with FEM results of Lourenco *et al.* (1999).

The results of the proposed coupled damage-homogenisation model are shown in Fig. 7b, where they are compared with the FE analysis of Lourenco *et al.* (1999) in the case with zero dilatancy angle. The damage model reproduces with good agreement the FE analysis of the cell degradation and the two peaks of the failure load. The head joint is the first to fail in tension and the bed joint takes its place in the load carrying mechanism of the cell. The load is transferred through bed joint shear from unit to the other, with the cell showing regained elastic behaviour for increasing loads, until final failure of the bed joint in shear. The residual load carrying capacity is zero because there is no vertical compression, and therefore no friction effect.

The homogenisation model was also tested in the simulation up to failure of a basic masonry cell under axial compressive loading perpendicular to the bed joint. For this problem numerical results are available from the accurate FE calculations of Pina-Henriques and Lourenço (2003) in the case of a masonry cell with solid soft-mud bricks of dimensions 250×120×55 mm^3 and mortar joint thickness of 10 mm. These FE analyses, aimed at the simulation of the deformation controlled tests of Binda et al. (1988), have been carried out with very detailed meshes either in plane stress, plane strain and enhanced plane strain with constant but non-zero normal strains in the out-of-plane direction, being the latter considered the closest possible plane representation of the three-dimensional behaviour. The non-linear behaviour of the cell components has been simulated by means of Drucker-Prager plasticity in compression and Rankine model or cracking in tension. Three different types of mortar were taken into consideration, namely weak and strong mortars.

The material data used by the homogenisation model are the same as in Pina-Henriques and Lourenço (2003). The axial stress *vs.* axial strain curves for one of the analysis (stronger mortar prism) is shown in Fig. 8. The curves obtained with the homogenisation model almost coincide with the corresponding FE results in enhanced plane strain, with marginal computational effort and no convergence difficulties. For weak mortars the plastic flow of the mortar joints starts very early in the loading path, while the brick non-linear behaviour begins a little later. The brick is in a tension-compression-tension state, while the mortar is in a tri-axial compression state for the lateral containment effect of the stiffer brick. The head joint suffers some negligible damage in tension just before the complete failure of the brick in tension, which leads to the catastrophic failure of the entire cell. For strong mortars the plastic flow starts earlier in the brick than in the bed joint, due to the higher strength of the mortar. The inversion of the elastic mismatch between mortar and brick in this case (the mortar is much stiffer than the brick) yields in this case a tension-tension-compression state of the bed joint. A substantial (57%) isotropic damage in tension is reached in the bed joint, but the failure of the masonry cell is driven again by the crushing of the brick. The damage of the mortar in the bed is due to the high tension in the x and z direction.

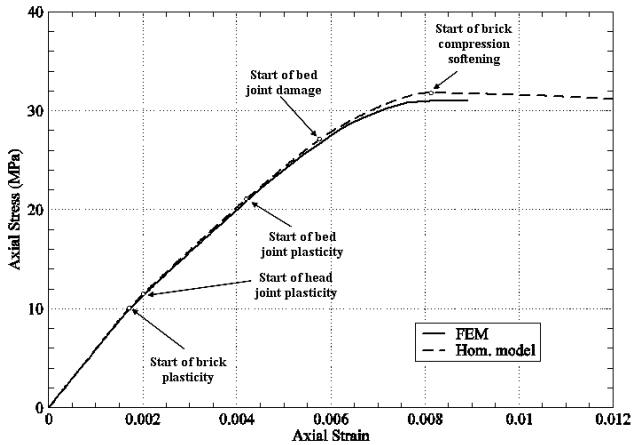

Figure 8 : Axial stress vs. axial strain for stronger mortar (prism MU3). Comparison between finite element simulation (Pina-Henriques and Lourenço, 2003) and non-linear homogenisation model.

4 A STRESS FIELD EXPANSION APPROACH

Fig. 9 presents a masonry wall Ω constituted by a periodic arrangement of bricks and mortar disposed in running bond texture, together with a rectangular periodic R.V.E. As shown in a classical paper by Suquet (1983), homogenization techniques combined with limit analysis can be applied for an estimation of the homogenized strength domain S^{hom} of masonry.

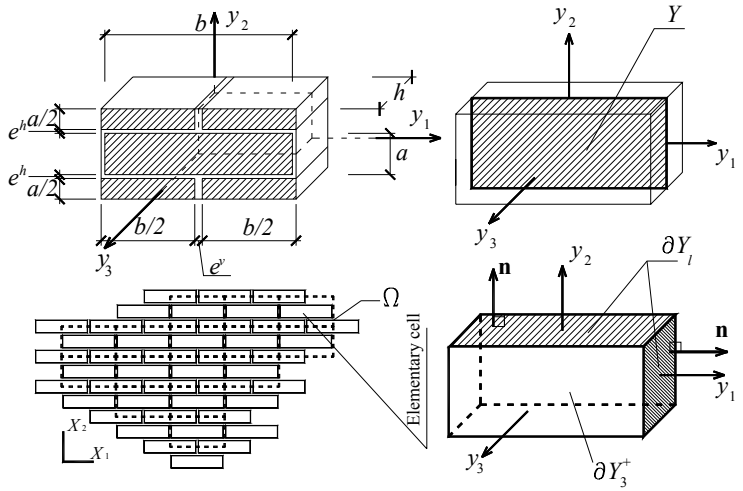

Figure 9 : Periodic structure ($X_1 - X_2$ macroscopic frame of reference) and R.V.E. ($y_1 - y_2 - y_3$ local frame of reference).

In this framework, bricks and mortar are assumed rigid-perfectly plastic materials with associated flow rule. As the lower bound theorem of limit analysis states and under the hypotheses of homogenization, S^{hom} can be derived by means of the following (non-linear) optimization problem:

$$S^{\text{hom}} = \left\{ \Sigma \,|\, \left\{ \begin{array}{lll} \Sigma =< \boldsymbol{\sigma} >= \dfrac{1}{A}\displaystyle\int_Y \boldsymbol{\sigma} dY & & (a) \\ div\boldsymbol{\sigma} = \mathbf{0} & & (b) \\ [\![\boldsymbol{\sigma}]\!]\mathbf{n}^{\text{int}} = \mathbf{0} & & (c) \\ \boldsymbol{\sigma}\mathbf{n} \quad \text{anti - periodic} \quad \text{on} \quad \partial Y & & (d) \\ \boldsymbol{\sigma}(\mathbf{y}) \in S^m \quad \forall \mathbf{y} \in Y^m \;;\; \boldsymbol{\sigma}(\mathbf{y}) \in S^b \quad \forall \mathbf{y} \in Y^b & & (e) \end{array} \right. \right\} \tag{21}$$

Here, $[\![\boldsymbol{\sigma}]\!]$ is the jump of micro-stresses across any discontinuity surface of normal $\mathbf{n}^{\text{int}}$. Conditions (21a,d) are derived from periodicity, condition (21b) imposes the micro-equilibrium and condition (21e) represents the yield criteria for the components (brick and mortar). The averaged quantity representing the macroscopic stress tensors $\boldsymbol{\Sigma}$ is given by:

$$\boldsymbol{\Sigma} =< \boldsymbol{\sigma} >= \frac{1}{A}\int_Y \boldsymbol{\sigma} dY \tag{22}$$

where A stands for the area of the elementary cell, $\boldsymbol{\sigma}$ stand for the local stress quantity and <*> is the averaging operator.

The proposed solution approach involves a simple and numerically suitable approach for solving the optimization problem. As shown in Fig. 10a, one-fourth of the R.V.E. is sub-divided into nine geometrical elementary entities (sub-domains), so that all the cell is sub-divided into thirty-six sub-domains, as shown in Fig. 10b. The subdivision adopted is the coarser (for ¼ of the cell) that can be obtained using rectangular geometries for every sub-domain. The macroscopic behaviour of masonry strongly depends on the mechanical and geometrical characteristics both of units and vertical/horizontal joints. For this reason, the subdivision adopted seems to be also particularly attractive, giving the possibility to characterize separately every component inside the elementary cell. For each sub-domain, polynomial distributions of degree *m* are a pri-

ori assumed for the stress components. Since stresses are polynomial expressions, the generic ij^{th} component can be written as follows:

$$\sigma_{ij}^{(k)} = \mathbf{X}(\mathbf{y})\mathbf{S}_{ij}^{T} \quad \mathbf{y} \in Y^k \tag{23}$$

where:

$\mathbf{X}(\mathbf{y}) = \begin{bmatrix} 1 & y_1 & y_2 & y_1^2 & y_1 y_2 & y_2^2 & \dots \end{bmatrix}$;

$\mathbf{S}_{ij} = \begin{bmatrix} S_{ij}^{(1)} & S_{ij}^{(2)} & S_{ij}^{(3)} & S_{ij}^{(4)} & S_{ij}^{(5)} & S_{ij}^{(6)} & \dots \end{bmatrix}$ is a vector of length ($\widetilde{N}$) ($\widetilde{N} = \frac{m^2}{2} + \frac{3m}{2} + 1 = \frac{(m+1)(m+2)}{2}$) representing the unknown stress parameters;

Y^k represents the k^{th} sub-domain.

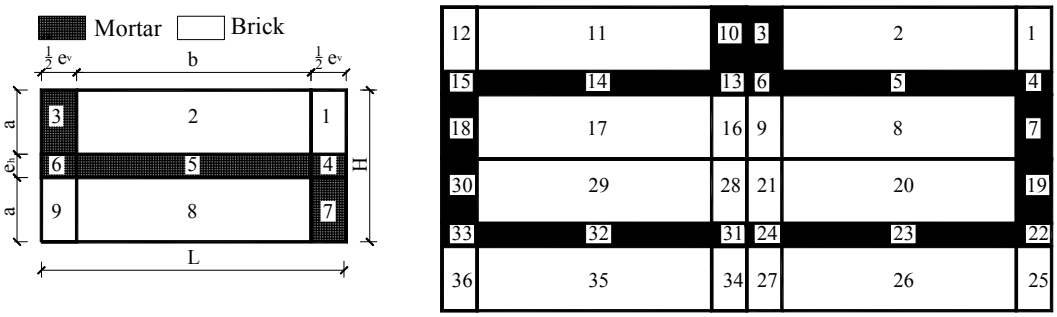

(a) (b)

Figure 10 : Adopted division in sub-domains: (a) subdivision and geometrical characteristics of one-fourth of the elementary cell; (b) subdivision into 36 sub-domains for the entire cell.

Cubic interpolation is recommended as an adequate degree for polynomial interpolation of the stress field. Details on equilibrium and anti-periodicity conditions, and validation of the approach are shown in Milani *et al.* (2006a,b). Extension of the formulation to out-of-plane behaviour is given in Milani *et al*. (2006c).

Again, the biaxial tests of Page (1981, 1983) are used for comparison. The panels were loaded proportionally in the principal stress directions Σ_h and Σ_v along different orientations ϑ with respect to the material axes. Both for mortar joints and units, a Mohr-Coulomb failure criterion in plane stress is adopted. It has to be emphasized that the experimental results provide only the mean compressive strength of mortar and bricks, insufficient for a full parametric identification of the model in plane stress. Furthermore, it should be underlined that the model at hand is only capable of reproducing the shape of the failure surface and not the actual strength in compression from the masonry components, since 3D effects are neglected and, in the framework of limit analysis, a ductile behavior of the bricks is assumed. For these reasons, mechanical characteristics of constituent materials are assumed with the aim of fitting experimental data. In Fig. 11 the homogenized failure surfaces for the orientation $\vartheta = 0°$, $\vartheta = 22.5°$ and $\vartheta = 45°$ are reported in comparison with experimental data, being in close agreement.

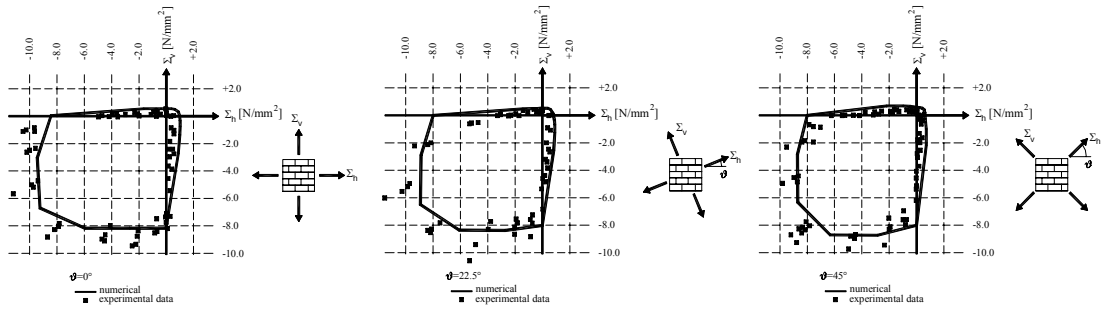

Figure 11 : Homogenized failure surface for Page (1981, 1983): (a) $\vartheta = 0°$; (b) $\vartheta = 22.5°$; (c) $\vartheta = 45°$.

4.1 Numerical results (in-plane)

The homogenised failure surface obtained with the above approach has been coupled with finite element limit analysis and applied to several examples of technical relevance. Both upper and lower bound approaches have been developed, with the aim to provide a complete set of numerical data for the design and/or the structural assessment of complex structures. The finite element lower bound analysis is based on the equilibrated triangular element by Sloan (1988), while the upper bound is based on a modified version of the triangular element with discontinuities of the velocity field in the interfaces by Sloan and Kleeman (1995). The modification takes into account the actual shape of the yield surface for the homogenised material in the interfaces. Several numerical simulations have been carried out in Milani et al. (2006b) in order to test the accuracy of the results obtained using homogenised finite element limit analysis.

Here, the clay masonry shear walls tested by Ganz and Thürlimann (1984) at ETH Zurich and analysed in Lourenço (1996) is reported. The geometry of the walls is depicted in Fig. 12a. The dimension of the bricks is assumed to be 300×200×150 mm^3, whereas the thickness of joints is supposed infinitesimal. Vertical flanges have the width of a single unit and a distributed vertical load P = 415 kN is applied on the rigid RC beam on the top. Both for mortar joints and units, a Mohr-Coulomb failure criterion in plane stress is adopted. Experimental evidences show a very ductile response, see Fig. 12b, so justifying the use of limit analysis for predicting the collapse load, with tensile and shear failure along diagonal stepped cracks.

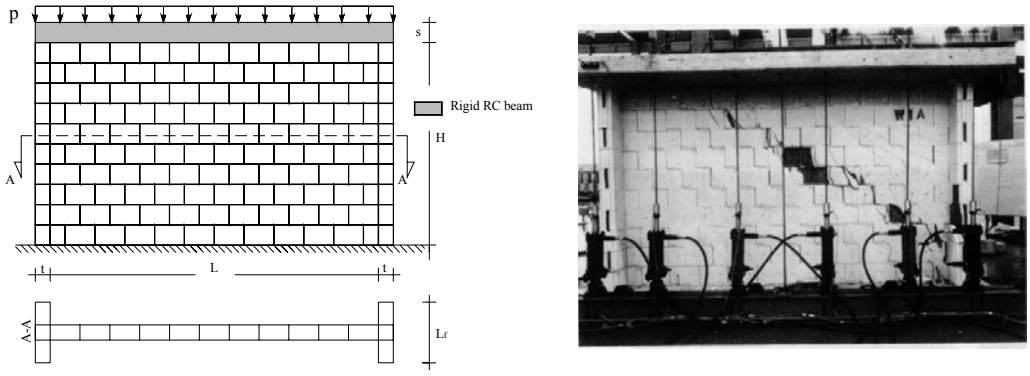

(a) (b)

Figure 12 : ETH Zurich shear wall: (a) geometry and loads (L= 3300 mm; t=150 mm; s=160 mm L_f=300 mm); (b) failure pattern.

In Fig. 13a,b the principal stress distribution at collapse from the lower bound analysis and the velocities at collapse from the upper bound analysis are reported. Good agreement is found among the model here proposed, the incremental elastic-plastic analysis reported in Lourenço (1996) and experimental data. Finally, in Fig. 13c a comparison between the numerical failure loads provided respectively by the lower and upper bound approaches and the experimental load-displacement diagram is reported. Collapse loads P(–) = 210 kN and P(+) = 245kN are numerically found using a model with 288 triangular elements, whereas the experimental failure shear load is approximately P = 250 kN.

4.2 Numerical results (out-of-plane)

Milani et *al.* (1996c) further extended and validated the formulation of the previous section to out-of-plane loading. The elementary cell is subdivided along the thickness in several layers. For each layer, fully equilibrated stress fields are assumed, adopting polynomial expressions for the stress tensor components in a finite number of sub-domains, imposing the continuity of the stress vector on the interfaces and defining anti-periodicity conditions on the boundary surface. Furthermore, admissibility constraints are imposed for the constituent materials enforcing the satisfaction of the yield conditions for joints and bricks on a regular grid of points. The out-of-plane failure surfaces of masonry obtained are implemented in FE limit analysis codes (both upper and lower bound) for structural analyses at collapse of entire panels.

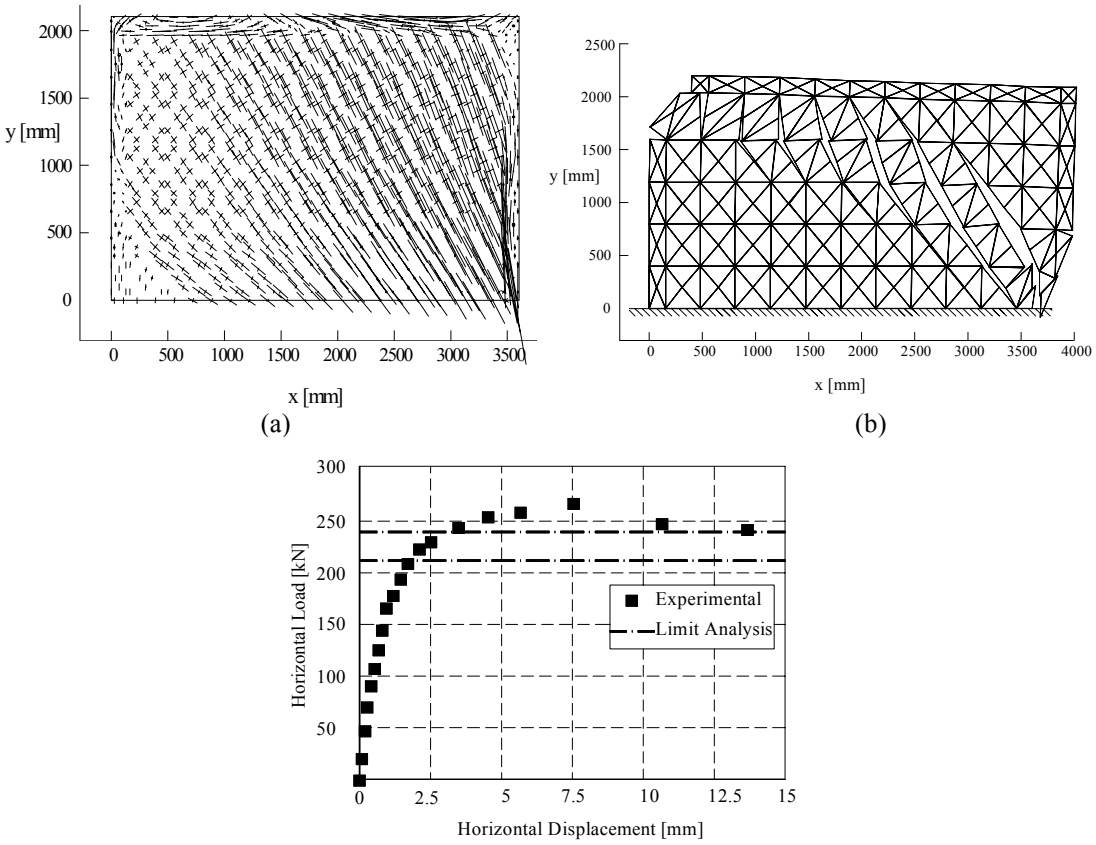

Figure 13 : Results from masonry shear wall:. (a) Principal stress distribution at collapse from the lower bound analysis; (b) Velocities at collapse from the upper bound analysis; (c) Comparison between experimental load-displacement diagram and the homogenised limit analysis (lower bound and upper bound approaches).

The ability of the homogenization procedure proposed to reproduce the strength of different masonry walls subjected to out-of-plane loads is tested for different orientations ϑ of the bending moment with respect to the bed joint direction is assessed next. A complete set of experimental strength data for specimens subjected to out-of-plane loading is given by Gazzola *et al.* (1985) and Gazzola and Drysdale (1986), who tested 25 wallettes of hollow concrete block masonry, with different dimensions and with the bed joints making a variable angle with the direction of loading, in four-point bending.

In order to compare experimental data with the proposed model, mechanical properties of mortar and bricks are taken in order to reproduce exactly the experimental value of f_{ft} reported by Gazzola and Drysdale (1986) for $\vartheta = 90°$. A comparison between experimental values and results from the numerical model for different orientation of the ϑ angle is given in Fig. 14, which shows the average and standard deviation of the tests for each orientation of loading.

The proposed homogenized model is also employed in order to reproduce experimental data for entire masonry panels out-of-plane loaded. As the current model assumes fully plastic behaviour, simple equilibrium equations, see Lourenço (2000), indicate that the experimental values of flexural tensile strength must be divided by three. The panels analyzed here consist of solid clay brick masonry. The tests were carried out by Chong *et al*. (1994) and Southcombe *et al.* (1995) and are denoted by SB. Four different configurations are tested, built in stretcher bond between two stiff abutments with the vertical edges simply supported (allowance for in-plane displacements was provided) and the top edge free. A completely restrained support was provided at the base because of practical difficulties in providing a simple support. The panels were loaded by air-bags until failure with increasing out-of-plane uniform pressure p.

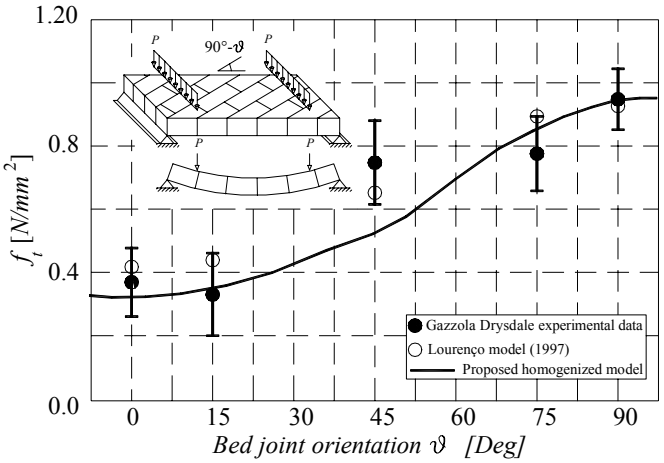

Figure 14 : Comparison between experimental results by Gazzola and Drysdale (1986), plasticity model by Lourenço (2000) and proposed model for the evaluation of flexural strength at different values of ϑ angle.

Fig. 15 shows typical comparisons between experimental pressure-displacement curves by Chong et al. (1995), numerical pressure-displacement curves obtained by means of an orthotropic elasto-plastic macro-model (Lourenço, 2000) and the new results with the proposed formulation. In addition, Fig. 16 shows typical results of the numerical analysis in terms of finite element mesh, principal moment distribution at failure, failure mechanisms and yield line pattern. The agreement with experimental results is worth noting in all cases analysed.

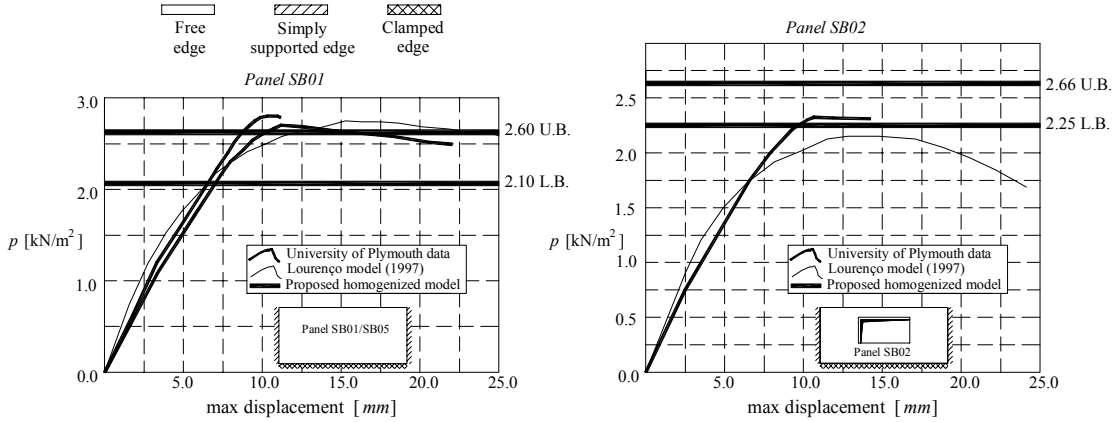

Figure 15 : Comparison between experimental and numerical results obtained, University of Plymouth experimental tests..

4.3 Numerical results (combined loading)

Finally, some real scale applications of the model to different buildings are shown in Fig. 17, demonstrating the possibility of using the proposed tools for the safety evaluation and strengthening of case studies efficiently. In particular, for the small building and by considering rather different material properties it is possible to find alternative collapse mechanisms that involve: (a) a combination of shear failure of transverse walls and overturning of façade; (b) a pure façade failure in out-of-plane bending with a vertical yield line at the centre of the wall and keeping the edges restrained; (c) global sliding at the base of the building. For the large building, a complex collapse mechanism involving piers and walls has been found.

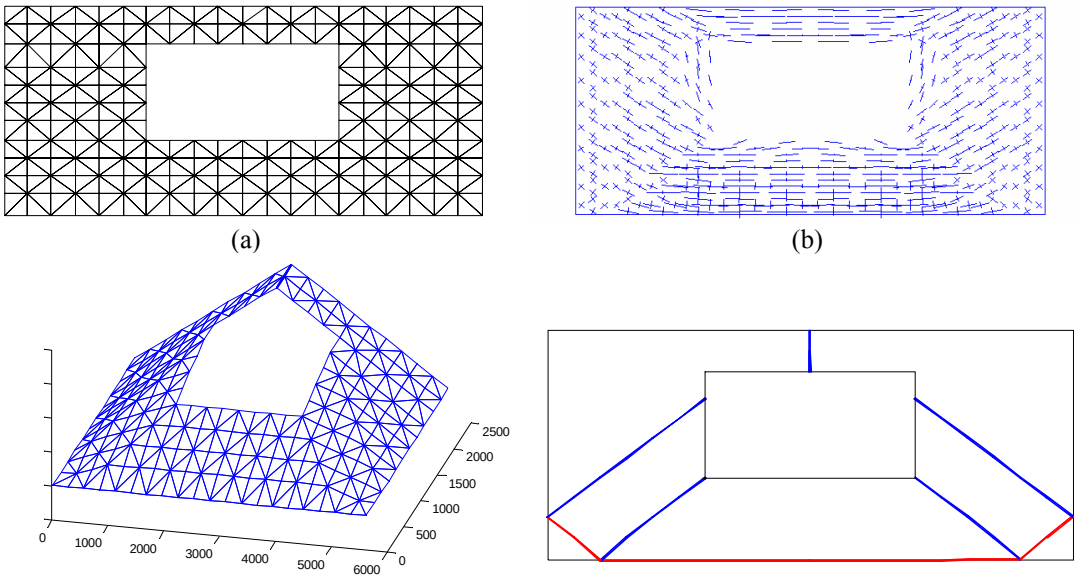

Figure 16 : Typical numerical results (Panel SB02): (a) homogenised finite element limit analysis mesh; (b) lower bound results (principal moments at collapse); (c,d) upper bound results (deformed mesh at collapse and yield line pattern)

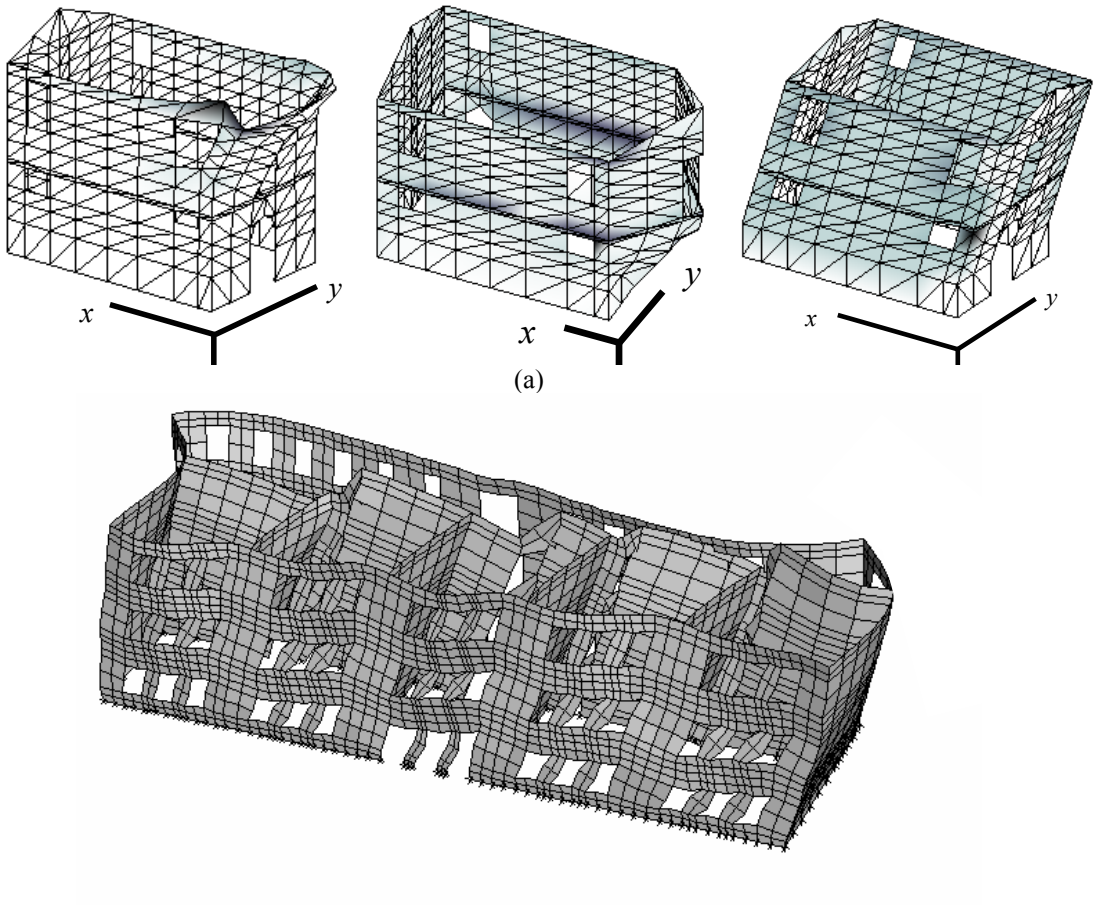

Figure 17 : Collapse mechanisms of buildings subjected to combined loading (vertical loading and seismic loading): (a) De Benedictis *et al.* (1991) house, including a sensitivity analysis leading to a set of possible failure modes; (b) Varano School, Ferrara, Italy.

5 CONCLUSIONS

Homogenisation techniques represent a popular and active field in masonry research. Several approaches have been recently introduced by different authors. Even if it impossible to predict the future of masonry research, this paper addresses two different approaches. The first approach is based on micromechanical deformation mechanisms coupled with standard finite element analysis. The second approach is based on a polynomial expansion of the stress field coupled with limit finite elements analysis. It is noted that both approaches, include a subdivision of the elementary cell in a high number of different sub-domains. In fact, very simplified division of the elementary cell, such as layered approaches, seems inadequate for the non-linear range.

Homogenised techniques based structural analysis is probably at a stage when it can start to compete with other structural analysis tools. In the case of limit finite element analysis, it seems that failure mechanisms and collapse loads similar to more complex approaches based on non-linear incremental and iterative finite element simulations. Such results are obtained at a very small fraction of the effort when compared to the non-linear simulations. Nevertheless, significant caution is always recommended when trying to reproduce existing damage patterns or define the safety level of existing masonry buildings using advanced non-linear simulations.

REFERENCES

Berto, L., Saetta, A., Scotta, R., Vitaliani, R. 2002, Orthotropic damage model for masonry structures. *International Journal for Numerical Methods in Engineering* 55(2), p. 127-157.

Binda L, Fontana A, Frigerio G. 1988. Mechanical behaviour of brick masonries derived from unit and mortar characteristics. In *Proc. 8th Int. Brick and Block Masonry Conf.*, Dublin.

Calderini, C., Lagomarsino, 2006. S., A micromechanical inelastic model for historical masonry. *Journal of Earthquake Engineering*, accepted for publication.

Chong, V.L., Southcombe, C., May, I.M. 1994. The behaviour of laterally loaded masonry panels with openings. In *Proc., 3th Int. Masonry Conf. Proc. Brit. Mas. Soc.*, London, p. 178-182.

CUR. 1997. *Structural masonry: An experimental/numerical basis for practical design rules*. Rots JG (ed). Balkema : Rotterdam.

De Benedictis R., de Felice G., Giuffrè A. 1991. In Giuffrè A (ed.), *Safety and conservation of historical centres: the Ortigia case*. Chapter 9: Seismic Retrofit of a Building, p. 189-217.

Dhanasekar, M., Page, A.W., Kleeman, P.W. 1985. The failure of brick masonry under biaxial stresses. *Proceedings from the Institution of Civil Engineers - Part 2* 79, p. 295-313.

Ganz, H.R., Thürlimann, B. 1984. Tests on masonry walls under normal and shear loading (in German). Report No. 7502-4. Institute of Structural Engineering, ETH Zurich : Zurich.

Gambarotta, L., Lagomarsino, S. 1997. Damage models for the seismic response of brick masonry shear walls. Part II: The continuum model and its applications. *Earthquake Engineering & Structural Dynamics* 26(4), p. 441-462.

Gazzola, E.A., Drysdale, R.G. 1986. A component failure criterion for blockwork in flexure. In S.C. Anand (ed.), Structures ‘86 ASCE, New Orleans, p. 134-153.

Gazzola, E.A., Drysdale, R.G., Essawy, A.S. 1985. Bending of concrete masonry walls at different angles to the bed joints. In *Proc. 3th North. Amer. Mas. Conf.*, Arlington, Paper 27.

Lopez, J., Oller, S., Oñate, E., Lubliner, J. 1999. A homogeneous constitutive model for masonry. *International Journal for Numerical Methods in Engineering* 46, p. 1651-1671.

Lourenço P.B. 1996. *Computational strategies for masonry structures*. PhD Thesis. Delft University of Technology : the Netherlands. Available from www.civil.uminho.pt/masonry.

Lourenço, P.B. 1998. Experimental and numerical issues in the modeling of the mechanical behavior of masonry. In Roca P et al. (ed.), *Structural analysis of historical constructions II*, p. 57-91. CIMNE : Barcelona.

Lourenço, P.B., Rots, J.G., Blaauwendraad, J. 1998. Continuum model for masonry: Parameter estimation and validation. *Journal of Structural Engineering, ASCE* 124(6), p. 642-652.

Lourenço, P.B., Rots, J.G., van der Pluijm, R. 1999. Understanding the tensile behaviour of masonry parallel to the bed joints: a numerical approach. *Masonry International* 12(3), p. 96-103.

Lourenço, P.B. 2000. Anisotropic softening model for masonry plates and shells. *Journal of Structural Engineering, ASCE* 126(9), p. 1008-1016.

Lourenço, P.B. 2002. Computations of historical masonry constructions. *Progress in Structural Engineering and Materials* 4(3), p. 301-319.

Maier, G., Papa, E., Nappi, A. 1991. On damage and failure of unit masonry. In: *Experimental and nu-*

merical methods in earthquake engineering, p. 223-245. Balkema : Brussels and Luxembourg.
Massart, T.J., Peerlings, R.H.J., Geers, M.G.D. 2004. Mesoscopic modeling of failure and damage-induced anisotropy in brick masonry. *European Journal of Mechanics A/Solids* 23, p. 719-735.
Milani, G., Lourenço, P.B., Tralli, 2006. A. Homogenised limit analysis of masonry walls. Part I: Failure surfaces. *Computers & Structures* 84(3-4), p. 166-180.
Milani, G., Lourenço, P.B., Tralli, A. 2006b. Homogenised limit analysis of masonry walls. Part II: Structural applications. *Computers & Structures* 84(3-4), p. 181-195.
Milani, G., Lourenço, P.B., Tralli, A. 2006c. A homogenization approach for the limit analysis of out-of-plane loaded masonry walls. *J. Struct. Engrg., ASCE*, accepted for publication.
Page, A.W. 1981. The biaxial compressive strength of brick masonry. *Proceedings from the Institution of Civil Engineers - Part 2* 71, p. 893-906.
Page, A.W. 1983. The strength of brick masonry under biaxial compression-tension, *International Journal of Masonry Construction* 3(1), p. 26-31.
Pande, G.N., Liang, J.X., Middleton, J. 1989. Equivalent elastic moduli for unit masonry. *Computers and Geotechnics* 8, p. 243-265.
Pietruszczak, S., Niu, X. 1992. A mathematical description of macroscopic behaviour of brick masonry. *International Journal of Solids and Structures* 29(5), p. 531-546.
Pina-Henriques J., Lourenço P.B. 2003. Testing and modelling of masonry creep and damage in uniaxial compression. *Proc. 8th STREMAH*, p. 151-160. WIT Press : Southampton.
Podestà, S.. 2005. A damage model for the analysis of the seismic response of monumental buildings. *Journal of Earthquake Engineering* 9(3), p. 419-444.
Rots, J.G. 1991. Numerical simulation of cracking in structural masonry, *Heron* 36(2), p. 49-63.
Sloan, S.W. 1988. Lower bound limit analysis using finite elements and linear programming. *International Journal for Numerical and Analytical Methods in Geomechanics* 12, p. 61-77.
Sloan, S.W., Kleeman, P.W. 1995. Upper bound limit analysis using discontinuous velocity fields. *Computer Methods in Applied Mechanics and Engineering* 127(1-4), p. 293-314.
Southcombe, C., May, I.M., and Chong, V.L. 1995. The behaviour of brickwork panels with openings under lateral load. In *Proc. 4th Int. Masonry Conf. Proc. Brit. Mas. Soc.*, London, p. 105-110.
Suquet, P. 1983. Analyse limite et et homogeneisation. *Comptes Rendus de l'Academie des Sciences - Series IIB – Mechanics* 296, p. 1355-1358. In French.
van der Pluijm, R. 1999. Out of plane bending of masonry: Behaviour and strength. Ph.D. Dissertation. Eindhoven University of Technology : The Netherlands.
Zucchini, A., Lourenço, P.B. 2002. A micro-mechanical model for the homogenization of masonry. *International Journal of Solids and Structures* 39, p.3233-3255.
Zucchini A, Lourenço P.B. 2004. A coupled homogenisation-damage model for masonry cracking. *Computer and Structures* 82, p. 917-929.
Zucchini A, Lourenço P.B. 2006. Mechanics of masonry in compression: Results from a homogenisation approach. *Computer and Structures*, accepted for publication.